Draft version February 19, 2009
Preprint typeset using LaTeX style emulateapj v. 10/09/06

THE DETECTION OF INSIDE-OUT DISK GROWTH IN M33

Benjamin F. Williams[1], Julianne J. Dalcanton[1], Andrew E. Dolphin[2], Jon Holtzman[3], Ata Sarajedini[4]

Draft version February 19, 2009

ABSTRACT

We present resolved stellar photometry of 4 fields along the major axis of the M33 disk from images taken with the Advanced Camera for Surveys aboard the Hubble Space Telescope. The photometry provides a detailed census of the red clump in all fields and reaches the ancient main sequence in the outermost field. Through detailed modeling of the color-magnitude diagrams, we find that the percentage of the stellar mass formed prior to $z = 1$ changes from 71±9% in the inner-most field to 16±6% in the outermost field. The disk shows a clear trend of increasing scale-length with time, evolving from $r_s = 1.0 \pm 0.1$ kpc 10 Gyr ago to $r_s = 1.8 \pm 0.1$ kpc at times more recent than 5 Gyr ago, in agreement with analytical predictions for disk growth. Beyond the disk truncation radius, however, the stellar density profile steepens with time and the age gradient reverses, in agreement with recent simulations. The late and slow growth of the stellar disk may be due in part to the low mass of M33.

Subject headings: galaxies: individual (M33) — galaxies: spiral — galaxies: evolution — galaxies: stellar content

1. INTRODUCTION

The scale-lengths of galaxy disks are thought to increase with time due to late time accretion of gas at large radii and exhaustion of gas in the centers of galaxies (Larson 1976; Matteucci & Francois 1989; Burkert et al. 1992; Chiappini et al. 1997; Naab & Ostriker 2006, and many others). This process, which has been called "inside-out" growth, reproduces many of the physical (e.g., Bouwens et al. 1997) and chemical properties of disks. Observations of color gradients in spiral galaxies suggest that the mean ages of the stars decrease from the inside-out (e.g., MacArthur et al. 2004), and observations of extended ultra-violet disks show that very recent star formation is prevalent in the outer regions of disks (e.g., Boissier et al. 2008). While these trends are consistent with inside-out growth, broadband colors can be biased by variations in star formation, dust extinction, and metallicity, while ultra-violet emission probes only the current disk properties. A more direct approach to detecting the products of long-term inside-out disk growth is through measurements of the age distribution of the resolved stellar populations.

The inside-out growth of stellar disks may be most easily detected in low-mass disks. If massive disks formed earlier than low-mass disks (i.e. "down-sizing" Cowie et al. 1996; Lilly et al. 2003; Neistein et al. 2006; Fontanot et al. 2009, and many others), the stars in massive disks have had more time to be mixed by radial redistribution processes (e.g., Roškar et al. 2008). Therefore detecting the signature of inside-out growth using stellar populations may be simplified in low-mass disks.

M33 is the nearest example of a low-mass disk galaxy. It is also a bulge-less system (McLean & Liu 1996), so that there is no confusion between disk and bulge populations. If the stellar disk of M33 grew from the inside-out, the age of the stellar populations should vary with radius, with a higher percentage of ancient stars in the inner disk. Indeed, ground-based observations of M33's bright stellar populations suggest that its outer disk may have formed at late epochs and may even be ongoing (Davidge 2003; Block et al. 2004; Rowe et al. 2005). On the other hand, M33 has a truncated disk (at r∼8 kpc, Ferguson et al. 2007) and the age of populations of the outer disk/halo show an age increase with radius based on HST/ACS data (Barker et al. 2007b,a), in contrast to the expectations of inside-out growth.

In this letter, we use data from the Hubble Space Telescope (HST) Advanced Camera for Surveys (ACS) to study the age distribution of the stellar populations of the M33 disk as a function of galactocentric radius. These distributions show a clear trend: regions nearer to the center formed a higher fraction of their stars at earlier times leading to a steady growth in the disk scale length. Our measurements therefore provide strong observational support for inside-out disk growth.

More rigorous checks of this analysis and more detailed studies of these fields will be provided in a future full-length paper (Holtzman et al. 2009, in preparation). We assume a distance of 800 kpc (Lee et al. 2002) for conversions of angular measurements to physical distances. We assume an inclination of 56° (Corbelli & Schneider 1997) for de-projections. We adopt a WMAP[5] cosmology for all conversions between time and redshift.

2. DATA ACQUISITION AND PROCESSING

We obtained HST/ACS imaging of 4 inner fields along the major axis of the M33 disk as part of the HST GO program 10190 (see left panel of Figure 1). The observations were performed from 09-Sep-2004 to 20-Feb-2005 through the F606W (wide-V) and F814W (I equivalent) filters. The total exposure time in the innermost field

[1] Department of Astronomy, Box 351580, University of Washington, Seattle, WA 98195; ben@astro.washington.edu; jd@astro.washington.edu
[2] Raytheon, 1151 E. Hermans Road, Tucson, AZ 85706; dolphin@raytheon.com
[3] Department of Astronomy, New Mexico State University, Box 30001, 1320 Frenger St., Las Cruces, NM 88003; holtz@nmsu.edu
[4] Department of Astronomy, University of Florida, 211 Bryant Space Science Center, PO Box 112055, Gainesville, FL, 32611; ata@astro.ufl.edu

[5] http://lambda.gsfc.nasa.gov/product/map/dr2/params/lcdm_wmap.cfm

was 6260 s and 6482 s in F606W and F814W, respectively. The total exposure time for each of the other 3 fields was 21140 s and 26300 s in F606W and F814W, respectively.

We also analyzed HST/ACS imaging of 3 outer fields along the minor axis of the M33 disk (GO-9479), which have been previously studied by Barker et al. (2007b). Our reanalysis of these fields allowed us to extend our radial profiles to larger radii and provided a consistency check between our analysis technique and those used for previous work.

Resolved stellar photometry was measured using the photometric pipeline of the ACS Nearby Galaxies Survey Treasury (Dalcanton et al. 2009). The pipeline uses the DOLPHOT (Dolphin 2000) software package to measure point spread function photometry and to determine errors and completeness as a function of color and magnitude using artificial star tests (Dalcanton et al. 2009; Williams et al. 2009). The final stellar catalogs contained 414780, 386894, 407741, and 309249 stars, from the innermost field to the outermost field, respectively. The resulting color-magnitude diagrams (CMDs) are shown in Figure 2. Our measurements of the Barker et al. (2007b) fields yielded 13522, 3958, and 1548 stars from the innermost field to the outermost field. The resulting CMDs were equivalent to those shown in Barker et al. (2007b).

The CMDs shown in Figure 2 qualitatively show the relative number of main sequence stars to giants increasing with the distance from the center of M33, suggesting decreasing stellar ages with increasing radius. To quantify this trend, we measured the star formation history (SFH) of each of the 4 fields using the software package MATCH (Dolphin 2002), which finds the best-fitting distribution of stellar ages and metallicities that reproduces the observed CMD assuming a Salpeter (1955) initial mass function (IMF) and the stellar evolution isochrones of Girardi et al. (2002) including recent updates (Marigo et al. 2008). The details of the fitting method used were the same as those employed in Williams et al. (2009), where results at old ages were binned to low time resolution to reduce errors and avoid over-interpreting details that could be due to deficiencies in the stellar evolution models. This technique for recovering the SFH from the CMD is well-tested and is found to be robust against differences in stellar evolution models and fitting techniques when the distance and mean extinction to the field are allowed to be fitted as free parameters.

Uncertainties were determined by fitting the CMDs with a range of assumed distance and mean reddening values. These uncertainties were then added in quadrature to the standard deviation calculated from Monte Carlo tests where the observed CMD was resampled and refitted one hundred times.

A constant mean extinction was applied to all model stars, using the ACS extinction coefficients from Girardi et al. (2008). Greater reddening was assumed for stars with ages <100 Myr, but these ages are not relevant to this study. As a first-order attempt to account for differential reddening, we applied a uniform spread in A_V to the model photometry of 0.6, 0.4, 0.2, and 0.0 magnitudes for the innermost to outermost fields (respectively). These values improved the quality of the model fits compared to fits with a single uniform reddening value for each field. However, differential reddening did not significantly alter the inferred SFHs (see § 3.4), which are shown in Figure 3.

3. RESULTS

3.1. *Star Formation Histories*

The M33 disk is naturally divided into two components: the inner disk and outer disk. These components are divided by a break in the exponential density profile located at a radius of ∼8 kpc (Ferguson et al. 2007). The radius of this truncation point is located between our outermost field and the innermost Barker et al. (2007b) field.

The SFHs of the fields (see Figure 3) show that the bulk of the stars in each ACS field formed at different times, as can be seen most easily by looking at the cumulative fraction of stars formed during each time bin. This value is plotted as a function of age for all 4 inner fields in the right panel of Figure 1. The plot clearly shows that, while the majority of the stars near the center of the disk had formed by $z = 1$, the bulk of the stars farther out in the disk formed later.

The growth is also shown in Figure 4, which plots the reconstructed stellar mass density profile of the M33 disk at 5 different epochs. This plot shows that most of the stellar disk growth occurred at radii of ∼3–7 kpc, rather than at the center, leading to an increase in the scale length of the inner disk (r<8 kpc) with little change in the central stellar surface density. In contrast, while the density profile of the inner disk has flattened as the disk has aged, that of the outer disk has steepened.

3.2. *Implications for the Inner Disk*

We have fit the inner disk (r<7 kpc) with an exponential profile and plotted the results in the central panel of Figure 4. The scale length of M33's disk has increased by a factor of ∼2 from 10 Gyr ago to the recent past. Most of this stellar disk growth occurred from 10 Gyr to 5 Gyr ago. This growth is similar to the predictions of Mo et al. (1998), which are based on simple scaling models for the evolution of the virial mass and virial radius.

The current stellar mass scale-length is longer than that of the K-band light (Regan & Vogel 1994, 5.8′ in K vs. 7.7′ here), suggesting a changing M/L_K with radius. This discrepancy has been seen in a dynamical estimate of the scale length of M33's mass (Ciardullo et al. 2004). However, the K-band scale length is similar to the scale length we calculate for stellar populations older than 5 Gyr.

The right panel of Figure 4 shows the extrapolated central surface density of the exponential fits to the stellar mass density profile. The uncertainties are significant, and the data are consistent with no evolution in the central surface density of the stellar disk (solid line). We compare the central surface densities with the expectations from the scaling laws of Mo et al. (1998); however, those laws track only the mean distribution of the baryons and formally predict a decrease in surface density with time. This prediction is not easily compared with our measurement for the *stellar* disk, for which such a decrease is likely to be unphysical.

Based on Figure 4, we conclude that most of the stars outside of the innermost field formed since $z =$

1. However, this conclusion differs from what has been seen in the outer disk of more massive spirals, such as M31 (Brown et al. 2006), M81 (Williams et al. 2009), and the Milky Way thick disk, in which most of the stars appear to have formed prior to $z = 1$. This early formation of the disks of massive spirals is also seen in redshift surveys, which are sensitive to equally massive spirals beyond $z = 1$ (Lilly et al. 1998; Ravindranath et al. 2004; Papovich et al. 2005; Sargent et al. 2007; Melbourne et al. 2007). Such surveys are not sensitive to low-mass disks like M33. The difference between our results for M33 and more massive disks may be due to the fact that such low-mass galaxies are thought to perform most of their star formation at later epochs, an effect that has been deemed "downsizing."

3.3. *Comparison to the Outer Disk*

There is a striking difference between the age gradient seen in our data for the inner disk and that seen in the far outer disk by Barker et al. (2007b). Within their series of outer disk fields, their measurements show the mean age of the stars increasing with radius. In contrast, our analysis shows the opposite effect within the break radius, marked by the vertical gray line in the left panel of Figure 4. Similar differences between the inner and outer disk are seen in current simulations of disk formation, where radial mixing redistributes older stars to larger radii. This mixing produces a break in the exponential disk profile, inside of which stellar ages decrease with increasing radius and outside of which stellar ages increase with increasing radius (Roškar et al. 2008). Although this radial mixing scatters stars into the outer disk, the majority of the stars in the inner disk remain close to their formation radius. Thus, while mixing produces the break and age gradient in the outer regions, it is not sufficient to erase the radial age gradient established during the formation of the inner disk.

Our independent reduction of the Barker et al. (2007b) data and derivation of the SFH reproduces their observed increase in mean age with radius in the outer disk. The resulting surface densities of these outer fields are included in Figure 4. Fits of a single exponential to the full broken exponential (see center panel of Figure 4) average the inner and outer disk gradient and thus show no significant change in scale-length with age. This exercise demonstrates the importance of measuring profiles of the disk inside and outside of the disk break separately.

Finally, our results show some very old stars at all radii in the disk. However, in disk formation and evolution simulations, radial redistribution places stars of the oldest ages throughout the disk, including much larger radii than where they were formed (Roškar et al. 2008), suggesting that the oldest stars seen at larger radii could have been formed closer to the galaxy center. The oldest stars may also have been accreted. In any case, the inner disk apparently had a shorter scale-length in the past, and the trends seen in mean age and scale-length in our measurements mimic those seen in simulations and semi-analytic models of inside-out growth.

3.4. *Reliability Tests*

Because our conclusions rely strongly on the reliability of our technique to measure SFHs from resolved stellar photometry, we have performed several tests to check the robustness of our measurements. Our conclusions draw upon the age distribution of stars with ages of 2-12 Gyr, resolved into 4 time bins. We performed multiple binnings to check the sensitivity of our results to binning scheme and verified that the same age gradient was present even for larger more conservative time bins than those finally adopted.

While such high time resolution in the 2-12 Gyr range is more robust at the depths of the outer 3 major axis fields, the ability to distinguish between stars with ages of 5 and 10 Gyr may be less reliable in the shallower innermost field. We therefore calculated the scale length of the inner disk as a function of time excluding the innermost field and found the trend to be equivalent to that measured when the innermost field is included.

We also tested the effects of forcing the distance to be the same in each fit by assigning a fixed distance of $(m - M)_0$=24.6 to all of the fields. This test decreased the scale lengths at all epochs, but left the trend the same.

The CMDs contain stars with a spread in reddening, such that the red clump appears slightly smeared along the reddening line. To test the effects of our assumption that differential reddening effects are less severe in fields farther out in the disk (see § 2), we refit our data first assuming the same spread in reddening ($A_V = 0.6$) in the innermost 3 fields and again assuming no differential reddening in any of the fields. While these changes affected the resulting overall scale lengths, causing the trend to be from 1.0±0.1 kpc to 1.7±0.2 kpc for a spread of $A_V = 0.6$ and from 1.1±0.1 kpc to 2.0±0.2 kpc for no spread at all, the changes did not significantly alter the resulting SFHs or change the trend of increasing scale length with time. More sophisticated tests of these effects will be reported in the more comprehensive paper on this dataset (Holtzman et al. 2009, in preparation).

We also checked for consistency with previous work. Our measured SFHs for the Barker et al. (2007b) fields were consistent with theirs within the errors except for a factor of ∼2 offset in the normalization, due to the IMF. Since Barker et al. (2007b) assumed an IMF that flattens at low masses, their models required lower star formation rates to reproduce the observed CMD. When normalized to produce the same number of stars from 1 to 100 $M_\odot$, the ratio of the total number of stars produced by their adopted IMF to that produced by our adopted IMF is ∼0.5. Correcting for this offset puts our resulting SFHs in good alignment with theirs. Changes in the IMF and mass cutoff serve only to shift all of the surface density data in Figure 4 up or down. The scale-lengths and fractional changes in central surface density are thus unaffected by these IMF issues, unless the true IMF varies with radius (Meurer et al. 2009).

4. CONCLUSIONS

We have modeled the CMDs of 7 HST/ACS fields in the M33 disk at a range of galactocentric radii. Four of these fields are newly-observed and lie along the major axis of the inner disk. The resulting stellar age distributions demonstrate that, within the inner disk, the age of the majority of the stars decreases with increasing distance from the galactic center. In addition, most of the disk stars outside of ∼3 kpc formed since $z = 1$,

later than what is seen in more massive spiral galaxies both in stellar populations studies and in redshift surveys. Comparisons of the stellar population properties in these fields with those of the outer M33 disk as measured by Barker et al. (2007b) show an inversion of the radial dependence of stellar age, providing support for some current simulation results. Together, these results provide strong observational support to inside-out growth of low-mass spiral stellar disks, down-sizing, and the significance of disk breaks in formation models of galaxy disks.

Support for this work was provided by NASA through grants GO-10190 and GO-10915 from the Space Telescope Science Institute, which is operated by the Association of Universities for Research in Astronomy, Incorporated, under NASA contract NAS5-26555.

REFERENCES

Barker, M. K., Sarajedini, A., Geisler, D., Harding, P., & Schommer, R. 2007a, AJ, 133, 1125
Barker, M. K., Sarajedini, A., Geisler, D., Harding, P., & Schommer, R. 2007b, AJ, 133, 1138
Block, D. L., Freeman, K. C., Jarrett, T. H., Puerari, I., Worthey, G., Combes, F., & Groess, R. 2004, A&A, 425, L37
Boissier, S., et al. 2008, ApJ, 681, 244
Bouwens, R. J., Cayon, L., & Silk, J. 1997, ApJ, 489, L21
Brown, T. M., Smith, E., Ferguson, H. C., Rich, R. M., Guhathakurta, P., Renzini, A., Sweigart, A. V., & Kimble, R. A. 2006, ApJ, 652, 323
Burkert, A., Truran, J. W., & Hensler, G. 1992, ApJ, 391, 651
Chiappini, C., Matteucci, F., & Gratton, R. 1997, ApJ, 477, 765
Ciardullo, R., Durrell, P. R., Laychak, M. B., Herrmann, K. A., Moody, K., Jacoby, G. H., & Feldmeier, J. J. 2004, ApJ, 614, 167
Corbelli, E., & Schneider, S. E. 1997, ApJ, 479, 244
Cowie, L. L., Songaila, A., Hu, E. M., & Cohen, J. G. 1996, AJ, 112, 839
Dalcanton, J. J., et al. 2009, ApJS, submitted
Davidge, T. J. 2003, AJ, 125, 3046
Dolphin, A. E. 2000, PASP, 112, 1383
Dolphin, A. E. 2002, MNRAS, 332, 91
Ferguson, A., Irwin, M., Chapman, S., Ibata, R., Lewis, G., & Tanvir, N. 2007, Resolving the Stellar Outskirts of M31 and M33 (Island Universes - Structure and Evolution of Disk Galaxies), 239
Fontanot, F., De Lucia, G., Monaco, P., Somerville, R. S., & Santini, P. 2009, ArXiv e-prints
Girardi, L., Bertelli, G., Bressan, A., Chiosi, C., Groenewegen, M. A. T., Marigo, P., Salasnich, B., & Weiss, A. 2002, A&A, 391, 195
Girardi, L., Dalcanton, J., Williams, B., de Jong, R., Gallart, C., Monelli, M., Groenewegen,M. A. T., Holtzman, J. A., Olsen, K. A. G., Seth, A. C., & Weisz, D. R. 2008, PASP, 120, 583
Larson, R. B. 1976, MNRAS, 176, 31
Lee, M. G., Kim, M., Sarajedini, A., Geisler, D., & Gieren, W. 2002, ApJ, 565, 959
Lilly, S., et al. 1998, ApJ, 500, 75
Lilly, S. J., Carollo, C. M., & Stockton, A. N. 2003, ApJ, 597, 730
MacArthur, L. A., Courteau, S., Bell, E., & Holtzman, J. A. 2004, ApJS, 152, 175
Marigo, P., Girardi, L., Bressan, A., Groenewegen, M. A. T., Silva, L., & Granato, G. L. 2008, A&A, 482, 883
Matteucci, F., & Francois, P. 1989, MNRAS, 239, 885
McLean, I. S., & Liu, T. 1996, ApJ, 456, 499
Melbourne, J., Phillips, A. C., Harker, J., Novak, G., Koo, D. C., & Faber, S. M. 2007, ApJ, 660, 81
Meurer, G. R., et al. 2009, arXiv:0902.0384
Mo, H. J., Mao, S., & White, S. D. M. 1998, MNRAS, 295, 319
Naab, T., & Ostriker, J. P. 2006, MNRAS, 366, 899
Neistein, E., van den Bosch, F. C., & Dekel, A. 2006, MNRAS, 372, 933
Papovich, C., Dickinson, M., Giavalisco, M., Conselice, C. J., & Ferguson, H. C. 2005, ApJ, 631, 101
Ravindranath, S., et al. 2004, ApJ, 604, L9
Regan, M. W., & Vogel, S. N. 1994, ApJ, 434, 536
Roškar, R., Debattista, V. P., Stinson, G. S., Quinn, T. R., Kaufmann, T., & Wadsley, J. 2008, ApJ, 675, L65
Rowe, J. F., Richer, H. B., Brewer, J. P., & Crabtree, D. R. 2005, AJ, 129, 729
Salpeter, E. E. 1955, ApJ, 121, 161
Sargent, M. T., et al. 2007, ApJS, 172, 434
Williams, B. F., et al. 2009, AJ, 137, 419

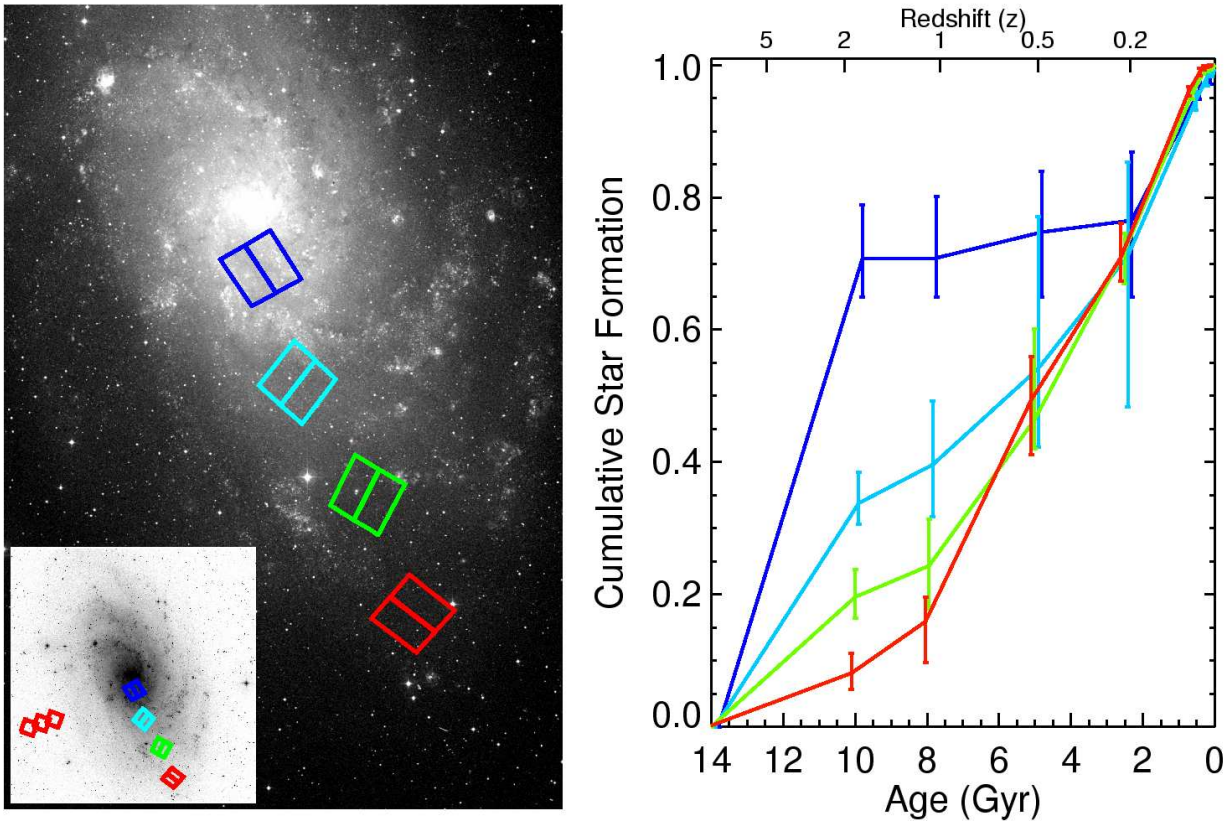

FIG. 1.— *Left:* A digitized sky survey image of M33. Overplotted in color are our 4 HST/ACS fields. The inset image shows the locations of the 3 Barker et al. (2007b) fields as red squares. *Right:* The cumulative fraction of stars formed in the four inner fields as a function of time. The colors of the lines are matched to the colors of the field outlines in *left*.

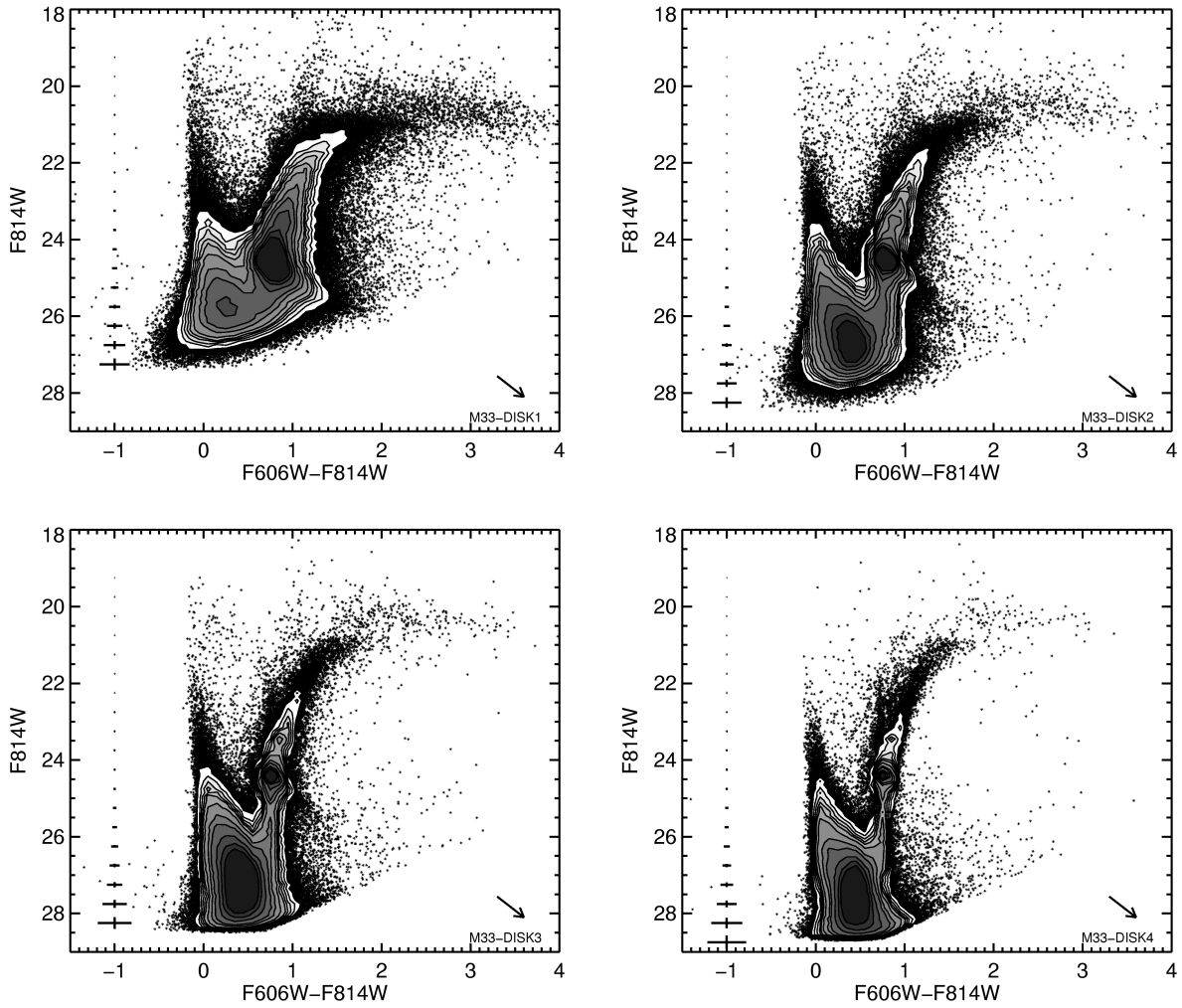

FIG. 2.— *Upper Left:* The F606W-F814W CMD of the innermost field. Contour levels indicate density of points where the plot would be saturated (levels are 1,1.5,2,2.5,3,4,6,8,12,16,20 $\times 10^4$ mag^{-2}). Photometric errors as a function of F814W magnitude are shown on the left side. The field name and reddening vector are shown in the lower-right corner. *Upper Right:* Same as *upper left*, for the next field out from the center. *Lower Left:* Same as *upper right*, for the next field out. *Lower Left:* Same as *lower left*, but for the outermost field. For CMDs of the archival fields, see Barker et al. (2007b).

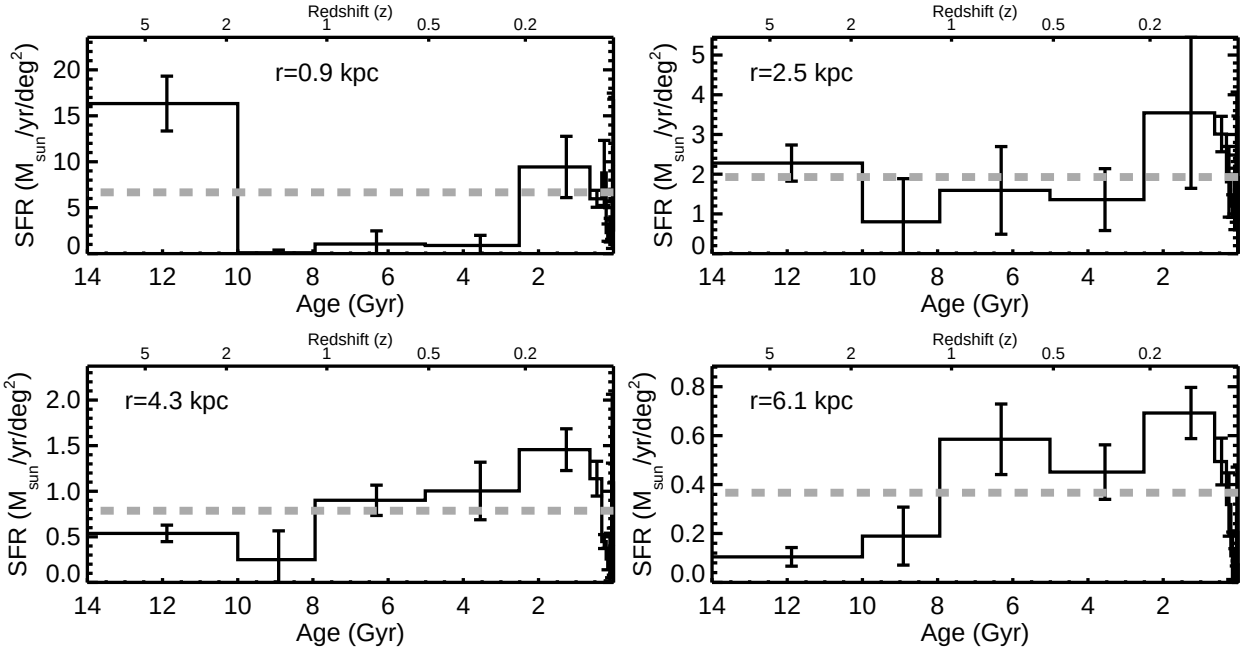

FIG. 3.— *Upper Left:* The star formation rate as a function of time of the innermost field. A thick, gray, dashed line denotes the mean rate for the field. *Upper Right:* Same as *upper left*, but for the next field out from the center. *Lower Left:* Same as *upper right*, but for the next field out. *Lower Left:* Same as *lower left*, but for the outermost field. For SFHs of the archival outer fields, please see Barker et al. (2007b).

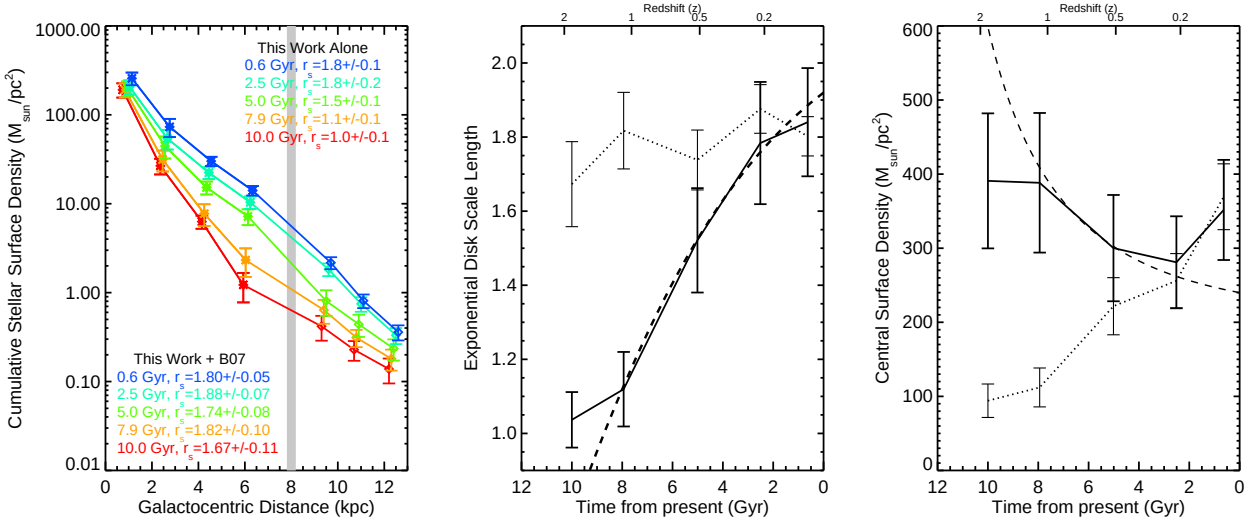

FIG. 4.— *Left:* M33 stellar surface densities as a function of de-projected radius as computed from our measured SFHs (stars) and from our re-analysis of the Barker et al. (2007b) fields (diamonds). Different colors show the total stellar densities that would be observed at different lookback times, noted in the corners. The absolute mass density values on the ordinate can shift based on the IMF. The best-fit exponential scale-length for each epoch using just the fields inside the disk break is listed in the upper-right. Those using all of the fields are listed in the lower-left. Data points have been offset from one another by 0.1 kpc to avoid overlapping error bars. The vertical gray line marks the disk break measured by Ferguson et al. (2007). *Center:* The disk scale length as a function of age inside the disk break (solid line) and from all fields (dotted line). The dashed line shows the scaling relation of Mo et al. (1998) normalized to our 5 Gyr measurement. *Right:* The central surface density as a function of age as measured from fields inside the disk break (solid line) and from all fields (dotted line). The dashed line shows the scaling relation of Mo et al. (1998) normalized to our 5 Gyr measurement.